Mercury sorption by silica/carbon nanotubes and silica/activated carbon: a comparison study

Tawfik A. Saleh

ABSTRACT

Nanocomposites of silica incorporated with carbon nanotubes (silica/CNT) and activated carbon (silica/AC) were synthesized and characterized by scanning electron microscopy (SEM), element mapping, energy dispersive X-ray spectroscopy (EDX), thermogravimetric analyzer (TGA) and Fourier transform infrared spectroscopy (FTIR). Silica/CNT and silica/AC were investigated for efficient removal of mercury ions from aqueous solutions. The adsorbents have been analyzed on the basis of adsorption capacity, reusability, and their application in packed columns. The effects of experimental parameters, like pH, contact time and initial concentrations on the adsorption of mercury ions, were optimized. The kinetic data for the adsorption process obeyed a pseudo-second-order kinetic model with R^2 of 0.999. Fitting the data to an intraparticle diffusion model indicated that surface adsorption and intraparticle diffusion were concurrently operating. In addition, this study used the Langmuir, Freundlich and Temkin isotherms to describe the behaviour of equilibrium adsorption. The equilibrium adsorption of the studied mercury ions is best fitted using the Freundlich isotherm, with silica/CNT of higher capacity than silica/AC. The silica/CNT showed better performance than silica/AC indicating silica/CNT has better efficiency.

Key words | adsorption, kinetics, mercury, nanocomposite

Tawfik A. Saleh
Chemistry Department,
King Fahd University of Petroleum & Minerals,
Dhahran 31261,
Saudi Arabia
E-mail: *tawfikas@hotmail.com*

INTRODUCTION

Mercury removal from wastewater has received significant attention due to its toxicity and thus high impact on the environment and public health. Adsorption technology, using ion-exchange resins, activated charcoal, nanomaterials and ion chelating agents immobilized on inorganic supports as adsorbents, is one of the most popular methods (Teng *et al.* 2011; Vasudevan *et al.* 2012; Wang *et al.* 2014; Mehdinia *et al.* 2015). Mercury is widely distributed in the environment from various sources including industries such as pigments, metallurgy, gilding copper, and instrumentation, oil, petrochemicals, recovery of gold, manufacture of chlorine and sodium hydroxide by electrolysis of brine and in many industries (Silva *et al.* 2010). The crude oil and liquid condensate can contain some quantities of mercury, ranging from nil to over 10 ppm. The mercury shortens the life of hydrogenation catalysts by deactivation and part of the mercury can also end up in the wastewater, causing contamination of the refinery site and, particularly, the wastewater treating facilities including the settling pond (Nasirimoghaddam *et al.* 2015).

Nanomaterials have wide applications as sorbents for water purification as they have high efficiency and capacity for heavy metal ions in aqueous solutions. Carbon-based nanomaterials have generated great interest in their use as adsorbents for the removal of pollutants from water/wastewater as they are stable, have limited reactivity, wide surface area, and are strong antioxidants (Halem *et al.* 2007; Peters *et al.* 2008; Sorlini & Gialdini 2014; Chawla *et al.* 2015; Naghizadeh 2015). For example, hybrid ligands-modified activated carbon, amine-modified activated carbon, multi-walled carbon nanotubes and chitosan/carbon nanotube composite beads (Zhu *et al.* 2009; Shadbad

doi: 10.2166/aqua.2015.050

et al. 2011; Shawky *et al.* 2012) have also been reported for their efficiency as adsorbents for mercury removal.

Because of their stability and large specific surface area, carbon nanotube (CNT) and activated carbon (AC) have attracted much attention (Saleh 2011; Gupta & Saleh 2013). On the other hand, silica has chemical stability and versatility in surface modification. Silica with different functionalities was studied as sorbents for pollutants sorption from waters (Chen *et al.* 2008; Yin *et al.* 2010).

Here, we report on the synthesis of silica/CNT and silica/AC and their sorption performance for mercury removal from aqueous solutions. The effects of contact time, initial concentration, pH and equilibrium isotherms on the process were investigated.

EXPERIMENTAL

Chemicals and materials

Carbon nanotubes (CNT) and activated carbon (AC) were prepared and activated as per the work reported earlier (Saleh 2011; Saleh & Al-Saadi 2015). The mercury standard stock solution (1,000 mg/L) Hg^{2+} was used. The solution was diluted to different initial concentrations as required. The initial pH of the tested solutions was adjusted to the desired value by using nitric acid or sodium hydroxide.

Synthesis of silica/CNT

Silica/CNT and silica/AC were prepared by dispersing CNT or AC in 0.1 L deionized water and 0.05 L ethylene glycol under ultrasonic vibration. Solution of 0.5 M of sodium meta silicate was prepared. The latter was added to the former under continuous stirring. The mixture was then kept under reflux at 120 °C under stirring (Saleh 2015). The composite was allowed to cool. It was then filtered, washed and dried at 100 °C. The possible interaction between silica and CNT or AC is proposed in Figure 1, step I.

Characterization and analysis

The prepared composites were characterized for the morphology using scanning electron microscopy (SEM) and element mapping, and structural properties using energy dispersive X-ray spectroscopy (EDX) and Fourier transform infrared spectroscopy (FTIR). A thermogravimetric analyzer (TGA) was used to evaluate the thermal stability of the prepared composites. Thermo Electron Corporation NXR FT-Raman module Nicolet 6700 FT-IR spectrometer in a region of 4,000–400 cm^{-1} was used to characterize the structure of the prepared silica/CNT and silica/AC. A thermal analyzer (STA 429) (Netzsch – Germany) at a constant heating rate of 10 °C/min under nitrogen flow was used to determine the thermal stability of the composites.

In order to specify the electrical neutrality of the adsorbent at a particular value of pH under aqueous solution conditions, point of net zero charge (pHzpc) was determined using the pH titration method. Briefly, 11 solutions with pH values of 1.0 to 12.0 were prepared. Then, 0.3 g of silica/CNT or silica/AC was added into each bottle and the final pH was measured after 48 h. The pH_{pzc} is defined as the point where the curve pH_{final} vs. $pH_{initial}$ crosses the line $pH_{final} = pH_{initial}$ (Órfão *et al.* 2006).

A mercury analyser was used to monitor the concentration of Hg^{2+} in the aliquots. Concentration of metal ions in real wastewater samples were monitored by inductively coupled plasma mass spectrometry (ICP-MS) model ICP-MS XSERIES-II Thermo Scientific with the following instrumental parameters; RF power 1,404 W, plasma gas flow 13 L/min, nebulizer gas flow 0.95 L/min, auxiliary gas flow 0.7 L/min, quartz pneumatic nebulizer, spray chamber: glass with peltier cooling, three replicates, acquisition mode; pulse counting, dwell time 10 ms, sweeps/reading 100 and acquisition parameters of scanning mode peak hopping, dwell time 300 ms and integration mode: peak area.

Sorption tests

The batch system

Specific amounts of silica/CNT or silica/AC were added into 20 mL of Hg^{2+} solution in plastic containers which were placed in a bath shaker at 150 rpm. The effect of the temperature was investigated by adjusting the temperature of the bath. Experimental parameters such as the effects of pH,

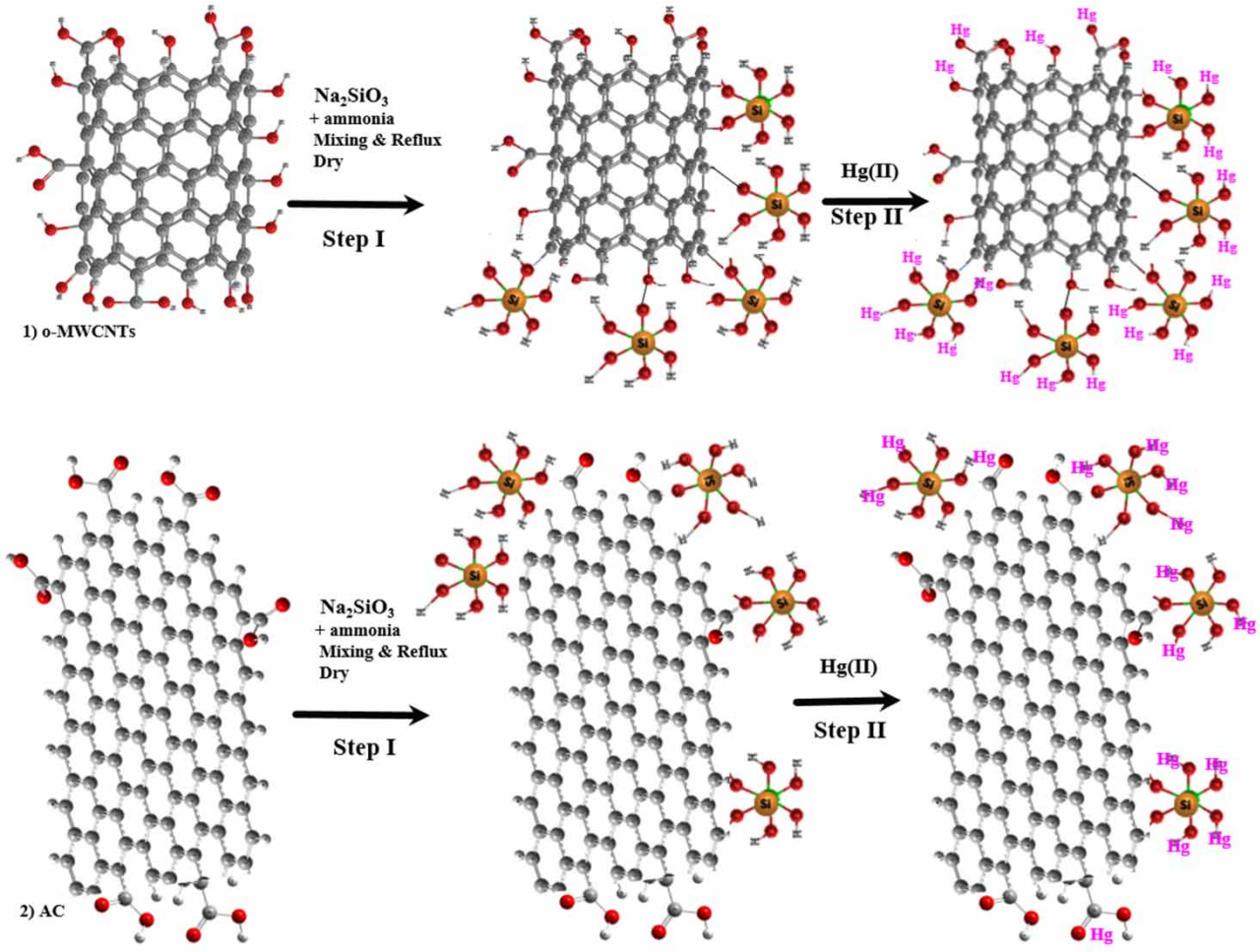

Figure 1 | Schematic illustration of silica /CNT and silica/AC preparation.

initial Hg^{2+} concentration, contact time and temperature were studied. A comparison was performed to evaluate the performance of the silica/CNT comparing with silica/AC. This study was conducted by adding an equivalent amount of each adsorbent into 20 mL of Hg^{2+} solution.

The fixed-bed system

The column was packed with the silica/CNT or silica/AC. Then the prepared Hg^{2+} solutions were passed through them in the bed to study their adsorption capacity. The column diameter and length used in every experiment was fixed constant. The different layer thickness of the adsorbent and the flow rate of the solutions were used as specified.

Recycling

The Hg-loaded silica/CNT or silica/AC were eluted by stirring with 1M HNO_3 to desorb Hg^{2+}. The silica/CNT or silica/AC was washed with de-ionized water and allowed to dry and then reused in adsorption processes.

Data analysis

The removal percentage (%) amounts of metal adsorbed per unit mass of adsorbent at equilibrium (q_e, mg/g) and at any time t (q_t, mg/g) were calculated by:

$$\%\,\text{Removal} = \frac{C_o - C_e}{C_o} \times 100 \quad (1)$$

$$q_t = (C_o - C_e) \times \frac{V}{m} \quad (2)$$

$$q_t = (C_o - C_t) \times \frac{V}{m} \quad (3)$$

C_o = initial mercury concentration in mg/L; C_t or C_e = concentrations at time or equilibrium in liquid phase.

RESULTS AND DISCUSSION

Characterization

The prepared silica/CNT or silica/AC were characterized for the morphology by field emission scanning electron microscopy (FESEM), and elemental mapping. Figure 2(a) depicts SEM image indicating nodes of silica nanoparticles on the nanotube surface. An elemental mapping image is presented in Figure 2(b) which indicates the uniform distribution of the elements, silica, carbon and oxygen in the silica/CNT. An EDX spectrum is depicted in Figure 2(c). The spectrum shows the elemental composition indicating the presence of carbon peak at 0.277 keV, oxygen at 0.525 keV and silica peak at 1.739 keV. The SEM image of silica/AC is given in Figure 3(a), which shows the morphology of the prepared materials with uniform elemental distribution as shown in Figure 3(b). The elemental composition of the sample indicated the presence of carbon peak at 0.277 keV, oxygen at 0.525 keV and silica peak at 1.739 keV with percent weight of each element as shown in Figure 3. TGA of the prepared silica/CNT or silica/AC showed that the silica/CNT has slightly more thermal stability than silica/AC, Figure 4. This can be attributed to the further interaction between nanotubes and silica compared with the interaction between activated carbon and silica (Yin *et al.* 2010; Zhang *et al.* 2010).

The IR spectrum, Figure 5, of the silica/CNT indicates the characteristic features of hydroxyl and carboxylic groups. The band at 1,720 cm^{-1} is assigned to stretching vibration of C = O in the carboxyl group. The band at 1,650 cm^{-1} is assigned to the carbonyl functional group while the band at 1,580 cm^{-1} is due to stretching vibrations of isolated C = C double bonds (Wang *et al.* 2009) and the band at 1,180 cm^{-1} (broad band 1,100–1,300 cm^{-1}) is assigned to the C-O stretching. Bands at 2,990 and 2,880 cm^{-1} are due to asymmetric and symmetric stretching of CH and are indicative of the presence of aliphatic -CH_2 groups. The broad peak at around 3,450 cm^{-1} indicates the generation of hydroxyl groups. The characteristic adsorption bands of silicon dioxide, the Si–O–Si asymmetric and symmetric stretching vibration at 1,080 and almost 800 cm^{-1}, respectively, and the O–Si–O symmetric bending vibration at 400–600 cm^{-1} (El-Gamel *et al.* 2011). The IR spectrum of the silica/AC shows lower structural properties than that of silica/CNT.

Sorption evaluation

Comparison

A comparison study was conducted by changing the type of adsorbent AC, CNTs, silica nanoparticles, silica/AC and silica/CNT for Hg^{2+} adsorption. As shown in Figure 6, the adsorption efficiency is in the order: AC < CNTs < silica < silica/AC < silica/CNT. The silica/CNT has better efficiency than silica/AC, which can be attributed to the better interaction between silica and nanotubes compared with activated carbon and silica, as seen in the cauterization section. On the other hand, the possible interaction between mercury ions and silica/CNT or silica/AC is proposed in Figure 1, step II.

Ph effect on Hg^{2+} adsorption

The effect of the pH of the solution on the mercury removal was studied. The results in Figure 7 indicate that while the silica/CNT showed better removal that silica/AC, both have the same trend. The mercury speciation distribution diagrams of mercury species at different pH values were considered for interpretation of the results (Zhang *et al.* 2005). The dominant species in the solution are Hg^{2+} at pH < 3.0, and $Hg(OH)_2$ at pH ≥ 6. Species $HgOH^+$, Hg^{2+}, $Hg(OH)_2$ are available in solutions of pH 3 to 6. The point of zero charge of the adsorbent was determined to be around 4. At pH ≤ 4, the surface of the adsorbents is relatively positive due to protonation, so the interaction or

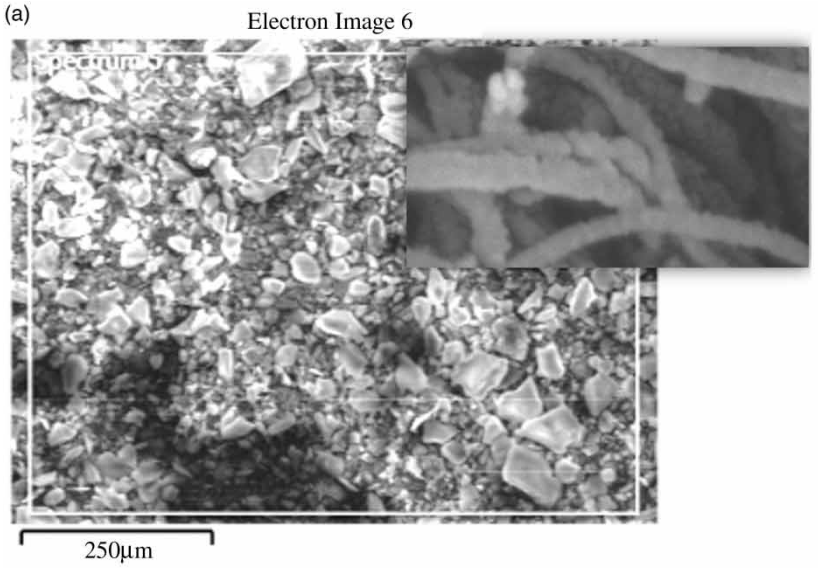

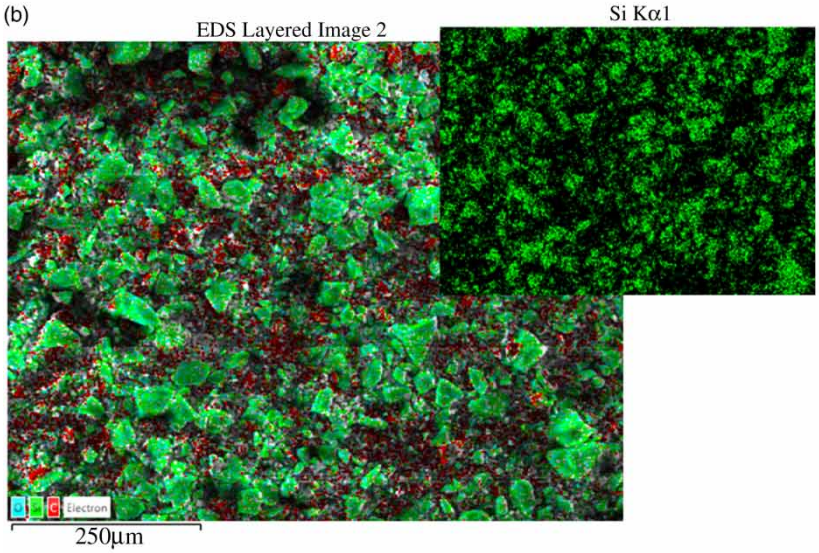

(c)

Element	Line Type	Apparent Concentration	k Ratio	Wt%	Wt% Sigma	Standard Label
C	K series	25.33	0.25335	51.36	0.90	C Vit
O	K series	34.73	0.11688	35.85	0.84	SiO2
Si	K series	22.80	0.18069	12.80	0.31	SiO2
Total:				100.00		

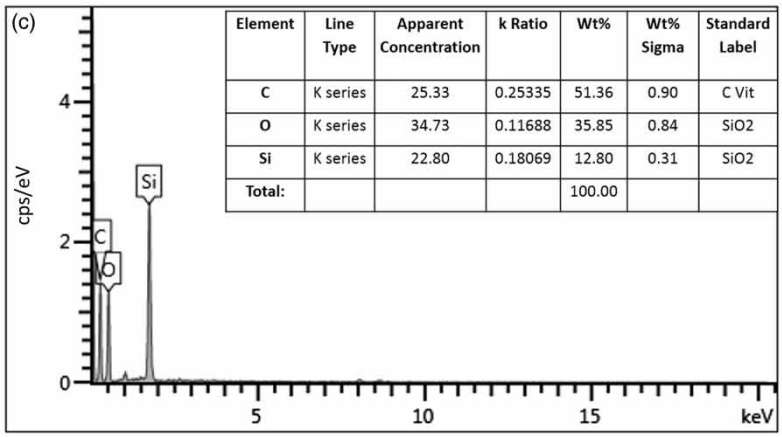

Figure 2 | SEM images, energy dispersive X-ray spectroscopy for elemental mapping (EDS) mapping and EDX spectrum of silica/CNT.

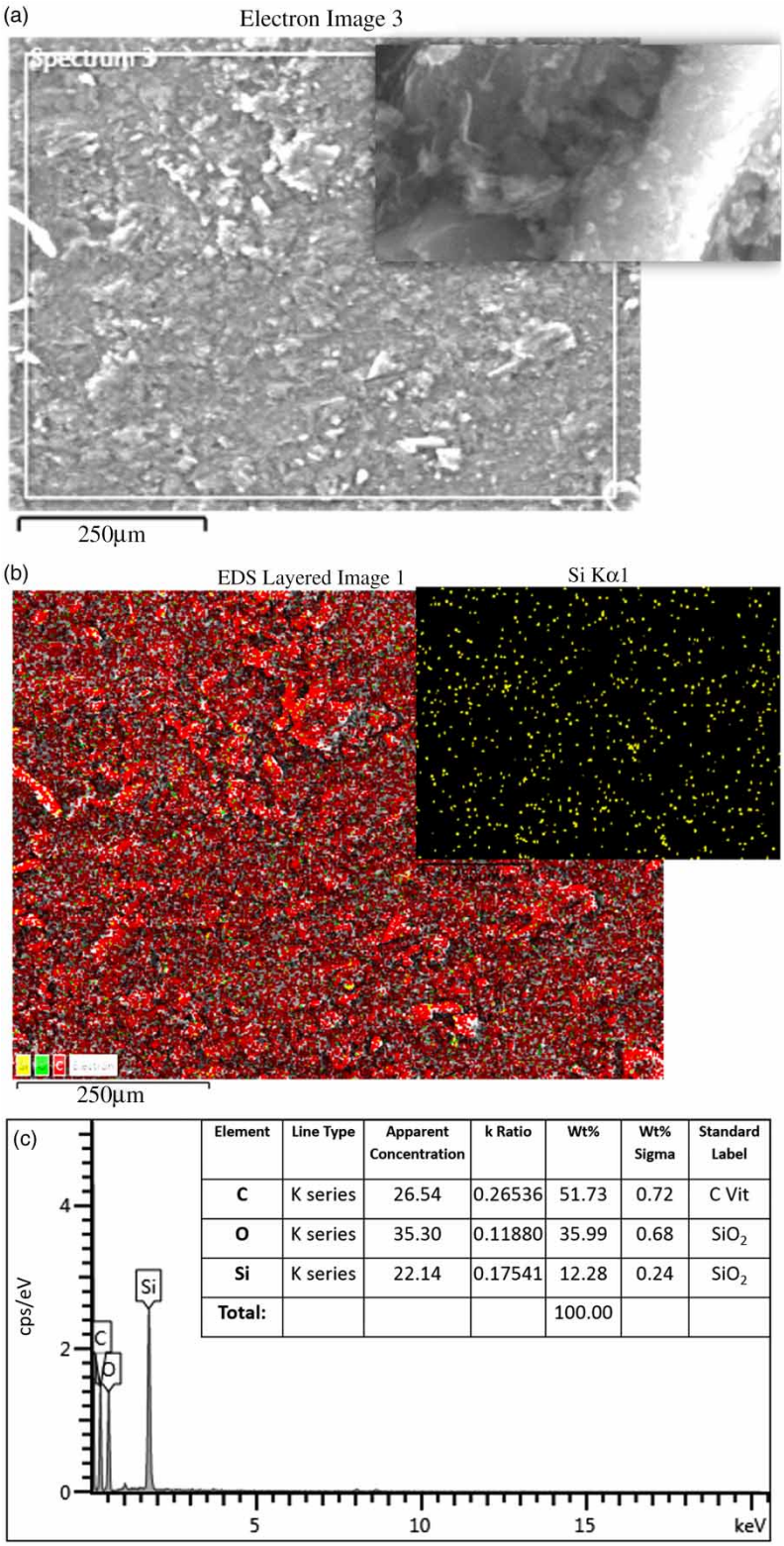

Element	Line Type	Apparent Concentration	k Ratio	Wt%	Wt% Sigma	Standard Label
C	K series	26.54	0.26536	51.73	0.72	C Vit
O	K series	35.30	0.11880	35.99	0.68	SiO_2
Si	K series	22.14	0.17541	12.28	0.24	SiO_2
Total:				100.00		

Figure 3 | SEM images, EDS mapping and EDX spectrum of silica/AC.

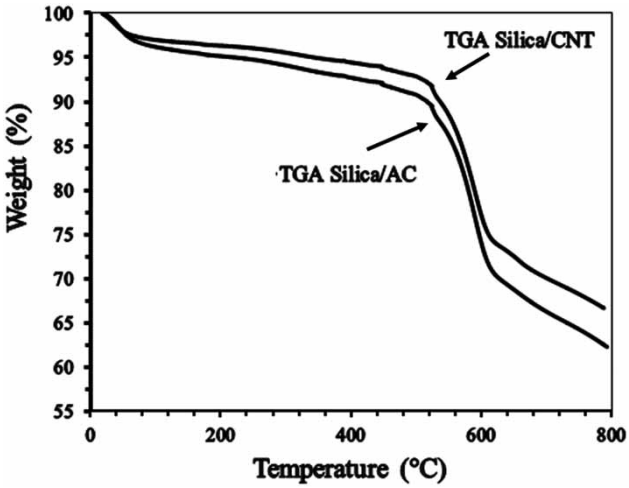

Figure 4 | TGA analysis of silica/CNT and silica/AC.

adsorption of mercury at pH values ≤4 is hindered by the repulsion as H^+ compete with mercury ions. At pH values >4, surface of the silica/CNT or silica/AC is negative due to deprotonation which enhances the interaction between the negatively charged surfaces and the Hg^{2+} ions.

Adsorption kinetic study

The pseudo-first-order, second-order kinetic models were used to express the mechanism of solute sorption onto a sorbent. In order to design a fast and effective model, investigations were made on adsorption rate. For the examination of the controlling mechanisms of adsorption process, such as chemical reaction, diffusion control and mass transfer, the intraparticle diffusion model was used to test the experimental data.

The following equation for pseudo-first-order kinetics was used (Lagergren 1898):

$$\ln (q_e - q_t) = \ln q_e - k_1 t \tag{4}$$

The following equation was used for pseudo-second order:

$$\frac{t}{q_t} = \frac{1}{k_2 q_e^2} + \frac{t}{q_e} \tag{5}$$

q_t and q_e = the amounts of Hg^{2+} in mg/g adsorbed at time t or equilibrium; k_1 and k_2 = rate constants.

The experimental data were plotted using the equations and the results are summarized in Table 1. It can be concluded that the adsorption process follows the pseudo-second order kinetic model and Hg^{2+} ions for both adsorbents, silica/CNT and silica/AC, Figure 8(a). This is supported by the good agreement of the equilibrium adsorption capacities ($q_{e,\,cal}$) with the experimentally observed data ($q_{e,\,exp}$) and the correlation coefficients of $R^2 > 0.99$.

The intraparticle diffusion coefficient, k_{id}, was determined by fitting the experimental data in the intraparticle diffusion model (Webber & Chakravarti 1974) using the following equation:

$$q_t = k_{id} t^{1/2} + C \tag{6}$$

k_{id} = intraparticle diffusion rate constant in mg/g.min$^{1/2}$; C = intercept in mg/g. The results obtained by the plot of q_t versus $t^{1/2}$ are listed in Table 1. The plots lines do not pass through the origin which indicates a degree of boundary layer control and this further indicates that the intraparticle diffusion is not the only rate-limiting step, but also other kinetic models may control the rate of adsorption.

Adsorption isotherms

The Langmuir, Freundlich and Temkin isotherm models were used. The Langmuir isotherm model assumes that a monolayer surface phase is formed on an energetically homogeneous surface of the adsorbent (Langmuir 1918). The following equation was used:

$$\frac{C_e}{q_e} = \frac{1}{k_L q_m} + \frac{C_e}{q_m} \tag{7}$$

where k_L = Langmuir equilibrium constant (litres/milligrams) related to the affinity of adsorption sites; q_m = maximum theoretical monolayer adsorption capacity in mg/g; C_e = equilibrium concentration in mg/L = ppm; q_e = amount of Hg^{2+} adsorbed at equilibrium in mg/g.

The characteristic parameter, R_L, known as separation factor, is defined by:

$$R_L = \frac{1}{1 + K_L C_o} \tag{8}$$

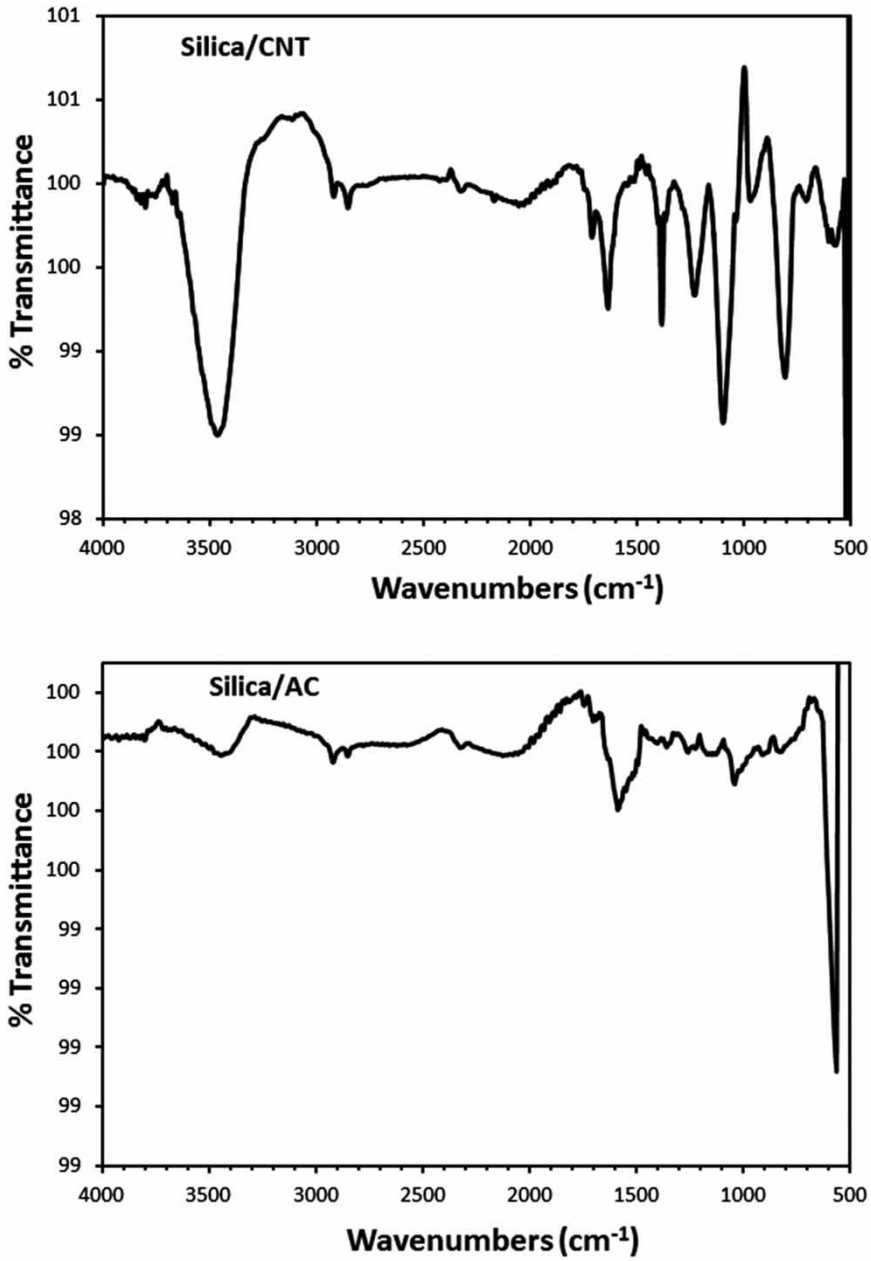

Figure 5 | FTIR spectrum of silica/CNT and silica/AC.

where C_o = initial mercury concentration. R_L provides an indication of the nature of the adsorption process.

The Freundlich model assumes a heterogeneous surface and takes into account the interactions between the adsorbed molecules (Freundlich 1906). The model of heterogeneous solids assumes a definite distribution of adsorption sites on the surface using:

$$\ln q_e = \ln K_f + \frac{1}{n} \ln C_e \quad (9)$$

where k_F = Freundlich isotherm constant (adsorption capacity) in mg/g; n = adsorption; C_e = equilibrium

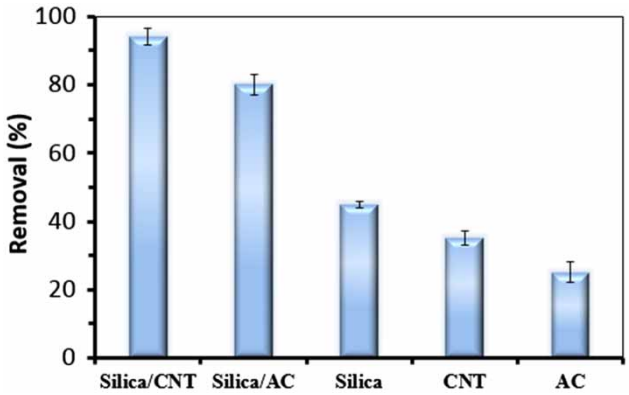

Figure 6 | Comparison between AC, CNTs, silica, silica/AC and silica/CNT for Hg^{2+} adsorption; initial concentrations of 40 ppm, dosage amounts 0.03 g, agitation speed 150 rpm, contact time 120 min.

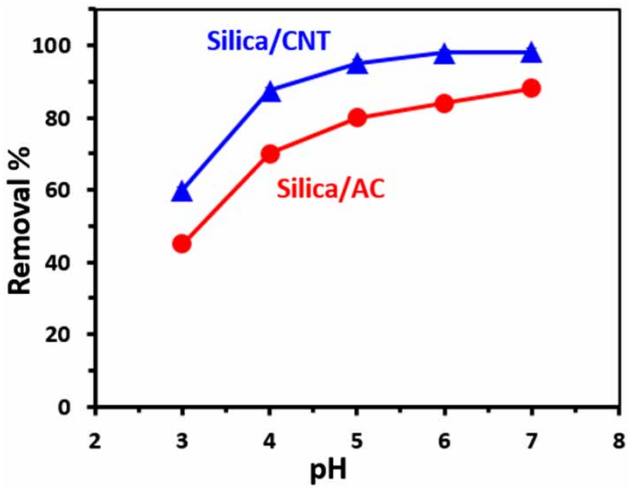

Figure 7 | Effect of pH on the adsorption of Hg^{2+} ions on silica/CNT and silica/AC.

concentration of adsorbate in mg/L; q_e = mg of mercury adsorbed per gram of the adsorbent.

The Temkin isotherm model considers the interactions between adsorbent and adsorbate. It assumes the adsorption energy in a layer decreases linearly with the surface coverage due to the interactions. It is expressed by:

$$q_e = \frac{RT}{b_T}\ln K_T + \frac{RT}{b_T}\ln C_e \quad (10)$$

where b_T = isotherm constant in joule per mole; k_T = isotherm equilibrium binding constant in L/g; R = gas constant 8.314×10^{-3} kJ/ mol.K; T = temperature in K.

The obtained results of models parameters are listed in Table 2. Considering the correlation coefficient (R^2), it can be observed that the experimental data fit better to the Freundlich isotherm, Figure 8(b), compared with the other models which means that the adsorption process are of heterogeneous surface with interactions between the adsorbed molecules. The value of k_f in the case of using silica/CNT is higher than silica/AC meaning that the silica/CNT is of better adsorption capacity than silica/AC. The n value gives an indication for the favourability of the adsorption process. The values of $n > 1$ represent a favourable adsorption condition. However, the value of n in the case of using silica/CNT is higher than silica/AC meaning that the silica/CNT is of more favourable adsorption condition than silica/AC.

Thermodynamic study

The thermodynamic parameters such as ΔG^0 (standard free energy), ΔH^0 (enthalpy change) and ΔS^0 (entropy change) have been estimated to determine the feasibility and the nature of adsorption process. The experimental data obtained at different temperatures were used in calculating the thermodynamic parameters. The values of ΔH^0 and ΔS^0 were calculated from the slopes and intercepts of the

Table 1 | Kinetic constant parameters obtained for Hg^{2+} adsorption on silica/CNT and silica/AC

			Lagergren's pseudo-first order			Pseudo-second order			Intraparticle diffusion model		
Adsorbent	**C_i (mg/L)**	**q_e, exp (mg/g)**	**k_1 (min^{-1})**	**q_e, cal (mg/g)**	**R^2**	**k_2[a]**	**q_e, cal (mg/g)**	**R^2**	**k_{id}[b]**	**C (mg/g)**	**R^2**
Silica/CNT	20	39	0.056	13	0.97	0.009	40	0.999	1.5	8	0.991
	40	76	0.053	38	0.93	0.003	80	0.998	1.1	12	0.980
Silica/AC	20	30	0.042	17	0.95	0.003	33	0.998	0.9	7	0.928
	40	58	0.03	36	0.83	0.001	63	0.995	0.8	9	0.949

[a](g/mg.min).
[b](mg/g.min).

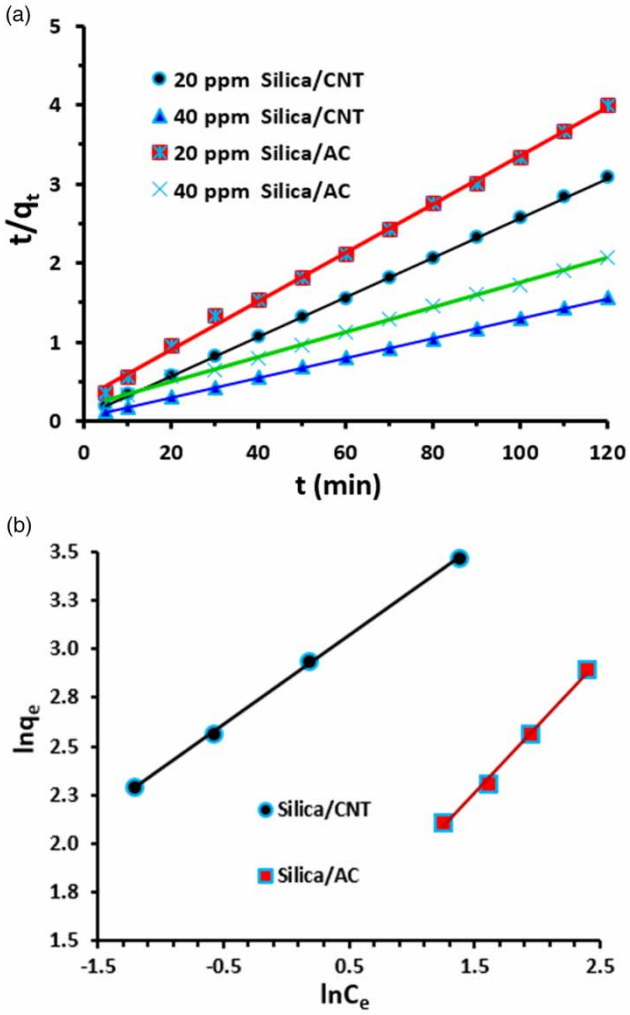

Figure 8 | Pseudo-second order kinetic plot (a) and Freundlich adsorption isotherm (b) for Hg^{2+} adsorption on Silica/CNT and Silica/AC.

plots of ln K_c versus $1/T$, for adsorption of Hg^{2+} on silica/CNT nanocomposite, by using the following linear Van't Hoff equation (Ghosh & Bhattacharyya 2002):

$$\ln K_c = \frac{\Delta S^0}{R} - \frac{\Delta H^0}{RT} \quad (11)$$

where R (8.314 kJ/mol.K) is the gas constant, T (K), absolute temperature and K_c (L/mg), standard thermodynamic equilibrium constant defined by q_e/C_e.

The free energy change $\Delta G^0 = \Delta H^0 - T\Delta S^0$ was calculated at 296, 316 and 336 K and was found to be –20, 21, 23 kJ/mol when silica/CNT was used and –13, 14, 16 kJ/mol when silica/AC was used. The decrease in its values with increasing temperature indicates the favorable adsorption at higher temperature. The positive standard enthalpy change ΔH^0 of 13 and 7 kJ/mol suggests the adsorption of Hg^{2+} is endothermic and the positive standard entropy change reflects the affinity of the adsorbents towards Hg^{2+}.

Desorption studies

The reusability of the silica/CNT and silica/AC is important in real applications from both an economic and environmental point of view. Therefore, reusability must produce a small volume of metal concentrate suitable for mercury recovery without damaging the adsorbent nature. Here, several cycles of alternating adsorption and desorption stages with silica/CNT or silica/AC were performed. Under the same selected operation conditions, the readsorption of Hg^{2+} reached percentages around 99% when silica/CNT was used, while it reached around 92% when silica/AC was used. This shows that the silica/CNT is highly effective for the adsorption of Hg^{2+} ions from aqueous solutions.

Bed column experiments

In this work, both silica/CNT and silica/AC were tested in a fixed bed column. The fixed bed column experiment was conducted with 10 ppm mercury solution at a bed depth of 10 cm and a constant flow rate of 3 mL/min. The breakthrough curve, Figure 9, was obtained. The silica/CNT showed

Table 2 | Langmuir, Freundlich and Temkin isotherms constants for Hg^{2+} adsorption on silica/CNT and silica/AC

	Langmuir isotherm				Freundlich isotherm				Temkin isotherm		
T (K)	q_m (mg/g)	k_L (L/mg)	R_L	R^2	1/n	n	k_f (mg/g)	$_R{}^2$	K_T (L/g)	b_T (KJ/mol)	$_R{}^2$
Silica/CNT	40	0.86	0.24	0.942	0.46	2.19	17	0.999	8.5	0.275	0.991
Silica/AC	34	0.08	0.15	0.914	0.69	1.45	3.3	0.995	1.5	0.288	0.968

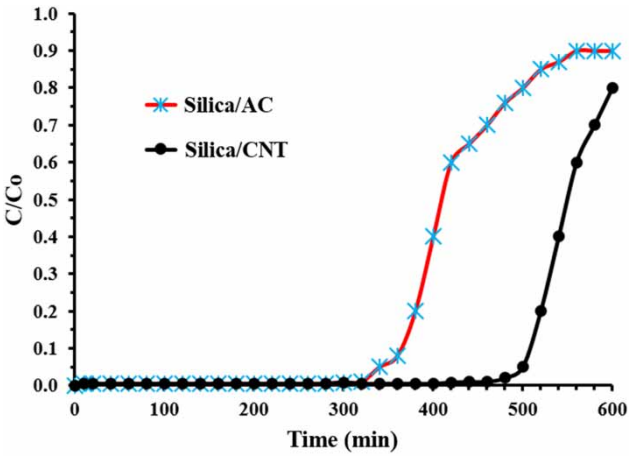

Figure 9 | Breakthrough curves of Hg^{2+} on the silica/CNT and silica/AC.

better performance than silica/AC with a breakthrough point at 500 min compared with 350 when silica/AC was used. This indicates that silica/CNT has better efficiency.

CONCLUSIONS

We reported the fabrication of silica/CNT and silica/AC. The prepared materials were characterized by SEM, element mapping, EDX and FTIR. The elemental mapping indicated the uniform distribution of the silica within the composite. The kinetic data for the adsorption process obeyed a pseudo-second-order kinetic model and Freundlich isotherm model, with silica/CNT of higher capacity than silica/AC. The finding confirms that intraparticle diffusion is involved in the adsorption process. The effectiveness of the silica/CNT was compared with silica/AC using a packed column for the removal of Hg^{2+}. The silica/CNT showed better performance with a longer breakthrough point than silica/AC. Therefore, the materials are promising candidates for heavy metal ion, especially mercury, removal. Further research on these adsorbents is required toward other pollutants.

ACKNOWLEDGEMENTS

Support from the Chemistry Department and King Fahd University of Petroleum and Minerals is gratefully acknowledged. The author would like to acknowledge the support provided by the Deanship of Scientific Research (DSR) at King Fahd University of Petroleum & Minerals (KFUPM) for funding this work through project No. JF121009.

REFERENCES

Chawla, J., Kumar, R. & Kaur, I. 2015 Carbon nanotubes and graphenes as adsorbents for adsorption of lead ions from water: a review. *J. Water Supply Res. Technol. AQUA* **64** (6), 641–659.

Chen, Q., Hills, C. D., Yuan, M., Liu, H. & Tyrer, M. 2008 Characterization of carbonated tricalcium silicate and its sorption capacity for heavy metals: A micron-scale composite adsorbent of active silicate gel and calcite. *J. Hazard. Mater.* **153**, 775–783.

El-Gamel, E. A., Wortmann, L., Arroubb, K. & Mathur, S. 2011 Sio2@Fe2O3 core–shell nanoparticles for covalent immobilization and release of sparfloxacin drug. *Chem. Commun.* **47**, 10076–10078.

Freundlich, H. 1906 Uber die adsorption in losungen (adsorption in solution). *Z. Phys. Chem.* **57**, 384–470.

Ghosh, D. & Bhattacharyya, K. 2002 Adsorption of methylene blue on kaolinite. *Appl. Clay Sci.* **20**, 295–300.

Gupta, V. K. & Saleh, T. A. 2013 Sorption of pollutants by porous carbon, carbon nanotubes and fullerene – an overview. *Environ. Sci. Pollut. Res.* **20**, 2828–2843.

Lagergren, S. 1898 About the theory of so-called adsorption of solution substances. *Kunglia Srenska Vertens Ka Psakademiens Handlingar* **24**, 1–39.

Langmuir, I. 1918 The adsorption of gases on plane surfaces of glass, mica and platinum. *J. Am. Chem. Soc.* **40**, 1362–1403.

Mehdinia, A., Akbari, M., Baradaran, T. & Azad, M. 2015 High-efficient mercury removal from environmental water samples using di-thio grafted on magnetic mesoporous silica nanoparticles. *Environ. Sci. Pollut. Res.* **22**, 2155–2165.

Naghizadeh, A. 2015 Comparison between activated carbon and multiwall carbon nanotubes in the removal of cadmium(II) and chromium(VI) from water solutions. *J. Water Supply Res. Technol. AQUA* **64** (1), 64–73.

Nasirimoghaddam, S., Zeinali, S. & Sabbaghi, S. 2015 Chitosan coated magnetic nanoparticles as nano-adsorbent for efficient removal of mercury contents from industrial aqueous and oily samples. *J. Ind. Eng. Chem.* **27**, 79–87.

Órfão, J. J. M., Silva, A. I. M., Pereira, J. C. V., Barata, S. A., Fonseca, I. M., Faria, P. C. C. & Pereira, M. F. R. 2006 Adsorption of a reactive dye on chemically modified activated carbons – influence of pH. *J. Colloid Interface Sci.* **296** (2), 480–489.

Peters, A. J., Weidner, K. L. & Howley, C. L. 2008 The chemical water quality in roof-harvested water cisterns in Bermuda. *J. Water Supply Res. Technol. AQUA* **57** (3), 153–163.

Saleh, T. A. 2011 The influence of treatment temperature on the acidity of MWCNT oxidized by HNO3 or a mixture of HNO3/H2SO4. *Appl. Surface Sci.* **257** (17), 7746–7751.

Saleh, T. A. 2015 Nanocomposite of carbon nanotubes/silica nanoparticles and their use for adsorption of Pb (II): from surface properties to sorption mechanism. *Desalination Water Treat.* 1–15, doi:10.1080/19443994.2015.1036784.

Saleh, T. A. & Al-Saadi, A. A. 2015 Surface characterization and sorption efficacy of tire-obtained carbon: experimental and semiempirical study of rhodamine B adsorption. *Surf. Interface Anal.* **47** (7), 785–792.

Shadbad, M. J., Mohebbi, A. & Soltani, A. 2011 Mercury(II) removal from aqueous solutions by adsorption on multi-walled carbon nanotubes. *Korean J. Chem. Eng.* **28**, 1029–1034.

Shawky, H. A., El-Aassar, A. & Abo-Zeid, D. E. 2012 Chitosan/carbon nanotube composite beads: Preparation, characterization, and cost evaluation for mercury removal from wastewater of some industrial cities in Egypt. *J. Appl. Polym. Sci.* **125**, E93–E101.

Silva, H. S., Ruiz, S. V., Granados, D. L. & Santángelo, J. M. 2010 Adsorption of mercury (II) from liquid solutions using modified activated carbons. *Mat. Res.* **13** (2), doi.org/10.1590/S1516-14392010000200003.

Sorlini, S. & Gialdini, F. 2014 Study on arsenic removal in the drinking water treatment plant of Cremona (Italy). *J. Water Supply Res. Technol. AQUA* **63** (8), 625–629.

Teng, M., Wang, H., Li, F. & Zhang, B. 2011 Thioether-functionalized mesoporous fiber membranes: Sol–gel combined electrospun fabrication and their applications for Hg2+ removal. *J. Colloid Interface Sci.* **355**, 23–28.

Van Halem, D., Heijman, S. G. J., Soppe, A. I. A., van Dijk, J. C. & Amy, G. L. 2007 Ceramic silver-impregnated pot filters for household drinking water treatment in developing countries: material characterization and performance study. *Water Sci. Technol. Water Supply* **7** (5–6), 9–17.

Vasudevan, S., Lakshmi, J. & Sozhan, G. 2012 Optimization of electrocoagulation process for the simultaneous removal of mercury, lead, and nickel from contaminated water. *Environ. Sci. Pollut. Res.* **19**, 2734–2744.

Wang, Z., Shirley, M. D., Meikle, S. T., Whitby, R. & Mikhalovsky, S. 2009 The surface acidity of acid oxidised multi walled carbon nanotubes and the influence of in-situ generated fulvic acids on their stability in aqueous dispersions. *Carbon* **47**, 73–79.

Wang, Q., Qin, W., Chai, L. & Li, Q. 2014 Understanding the formation of colloidal mercury in acidic wastewater with high concentration of chloride ions by electrocapillary curves. *Environ. Sci. Pollut. Res.* **21**, 3866–3872.

Webber, T. N. & Chakravarti, R. K. 1974 Pore and solid diffusion models for fixed bed adsorbers. *J. Am. Inst. Chem. Eng.* **20**, 228–238.

Yin, Z., Liu, X. & Su, Z. 2010 Novel fabrication of silica nanotubes using multi-walled carbon nanotubes as template. *Bull. Mater. Sci.* **33** (4), 351–355.

Zhang, M., Wu, Y., Feng, X., He, X., Chen, L. & Zhang, Y. 2010 Fabrication of mesoporous silica-coated CNTs and application in size-selective protein separation. *J. Mater. Chem.* **20**, 5835–5842.

Zhang, F., Nriagu, J. O. & Itoh, H. 2005 Mercury removal from water using activated carbons derived from organic sewage sludge. *Water Res.* **39**, 389–395.

Zhu, J., Deng, B., Yang, J. & Gang, D. 2009 Modifying activated carbon with hybrid ligands for enhancing aqueous mercury removal. *Carbon* **47**, 2014–2025.

First received 10 April 2015; accepted in revised form 6 July 2015. Available online 13 August 2015